

PAPER • OPEN ACCESS

Theoretical and experimental analysis of phase noise in semiconductor lasers biased below threshold

To cite this article: Iker Pascual de Zulueta and Angel Valle 2025 *J. Phys. Photonics* **7** 015013

View the [article online](#) for updates and enhancements.

You may also like

- [Apparent Diameters of F- to M-type Main-sequence Stars as Viewed from Habitable Zone Planets](#)
Shaan D. Patel, Manfred Cuntz and Nevin N. Weinberg
- [V442 Cen: Is the Accreting White Dwarf Ultra-rapidly Rotating?](#)
Laura Callahan, Edward M. Sion and Patrick Godon
- [Supernova Code Comparison: FLASH and Athena](#)
Breyton Ambler and Ryan Jeffrey Farber



PAPER

OPEN ACCESS

RECEIVED
30 September 2024REVISED
2 January 2025ACCEPTED FOR PUBLICATION
14 January 2025PUBLISHED
24 January 2025

Original Content from
this work may be used
under the terms of the
[Creative Commons
Attribution 4.0 licence](#).

Any further distribution
of this work must
maintain attribution to
the author(s) and the title
of the work, journal
citation and DOI.



Theoretical and experimental analysis of phase noise in semiconductor lasers biased below threshold

Iker Pascual de Zulueta and Angel Valle*

Instituto de Física de Cantabria, Universidad de Cantabria-CSIC, Santander, Spain

* Author to whom any correspondence should be addressed.

E-mail: valle@ifca.unican.es**Keywords:** semiconductor laser, optical phase, gain-switching, spontaneous emission noise, quantum random number generation, quantum key distribution

Abstract

We report a theoretical and experimental study of phase noise in semiconductor lasers when the bias current is below the threshold value. The theoretical study is performed by using two types of rate equations, with additive and multiplicative noise terms. We find the conditions for which the evolution in those rate equations can be described by 1-dimensional and two dimensional Brownian motions, respectively. The main statistical differences between the additive and multiplicative noise models are then illustrated by using the simplified Brownian motion models. Additive and multiplicative noise models predictions are compared with measurements of the phase noise with a coherent receiver using a 90° optical hybrid. We develop a novel method to extract the phase noise directly from our measurements, that in contrast to the usual direct method is not based on the analysis of the phase noise difference. The method permits a direct visualization of the phase noise trajectories and a calculation of the averages and the distribution that is valid in the short-time limit. Our results are in very good agreement with the results obtained with the method based on the phase noise difference. Our experimental results show that the variance of the phase noise grows linearly in time and has Gaussian statistics, supporting the modelization of the phase noise statistics with the additive noise model.

1. Introduction

The study of the fluctuations of the phase of the light emitted by semiconductor lasers has been a subject of interest since 1980s [1, 2]. Applications of single-frequency semiconductor lasers like coherent optical communications [2–4], coherent Lidar [5], high-resolution spectroscopy [6], and fiber-optic sensing [7] are behind that interest. In these applications the laser is mainly operated above its threshold current because a high degree of temporal coherence is required.

Phase fluctuations are also relevant in some recent applications of semiconductor lasers like quantum key distribution (QKD) [8, 9] and quantum random number generation (QRNG) [10]. QKD protocols provide information-theoretic secure communications based on the exchange of quantum states. Implementations of protocols typically rely on weak coherent pulses that usually consist of highly attenuated pulses generated by gain-switching semiconductor lasers. In this situation the performance of QKD is limited by multiphoton emissions for which an efficient solution, the decoy-state method, requires that the phases of all transmitted pulses are independent and uniformly random [11].

QRNGs use the inherent randomness of quantum mechanics to generate completely unpredictable random numbers with applications in QKD, Monte Carlo simulations, industrial testing, massive data processing, fundamental physics tests, etc [10, 12–14]. One of the most extended QRNGs, the so called phase noise QRNGs, are those based on gain-switching semiconductor lasers [9, 15–17]. These QRNGs have the advantages of fast operation, robustness and integration in photonic integrated circuits [18, 19].

In the above mentioned applications in QKD and QRNG semiconductor lasers are gain-switched from below to above their threshold current in order to generate trains of pulses with random phases. During the

below threshold operation the optical phase becomes random due to the effect of spontaneous emission noise that is a source of quantum randomness [20]. In this way characterization of phase fluctuations in the gain-switching operation is a problem worth studying.

To the best of our knowledge just a few measurements of phase fluctuations have been performed in the gain-switching regime [21, 22] or when the current is constant and below its threshold value [23]. Lovic *et al* measured the histogram of intensities at the output of an asymmetric interferometer and obtained the variance of the phase noise as the fitting parameter of that distribution [21]. Shakhovoy *et al* obtained the standard deviation of the phase noise, σ_φ , from the visibility of the pulse interference fringes [22]. In [23] σ_φ was obtained from the optical spectrum using the Schawlow-Townes law. A more direct way of measuring σ_φ is by using an offline digital coherent receiver [4]. In this method the variance of the phase noise is obtained from the average of the squared phase noise difference [4]. However, to our knowledge this method has only been used for constant bias currents above threshold because of its application in coherent communications.

Phase fluctuations have been theoretically described with two types of stochastic rate equations. The first one [24, 25] corresponds to that derived from first principles by Lax [26] and Henry [1] for a laser that is subject to a constant bias current. The noise terms in the photon number and phase equations are additive, so we will term this model as the additive noise model. In this way the phase evolution is analogous to that found in a 1-dimensional Brownian motion (1D-BM) and so the phase noise has a Gaussian distribution with a variance that increases linearly with time. The second type is considered when the laser is subject to a high-frequency modulation of the bias current. This type of modelling has been used in the analysis of phase noise QRNGs [9, 21, 22, 27–30] in which the laser is gain-switched with a switch-off current that is below the threshold value. The laser is in a transient regime and the exact form of the spontaneous emission noise terms is unknown [31]. In this modelling the averages of variables in the noise terms of the rate equations for photon number and phase are substituted by the corresponding variables. In this way those noise terms become multiplicative, so we will term this model as the multiplicative noise model. To the best of our knowledge this approximation has not been justified in a rigorous way. Although the use of this approximation has been successful for describing the experimental results relative to the transient statistics of quantities related to the laser power, like the first passage time [32], a problem appears when describing the phase statistics in the gain-switched regime with a below threshold switch-off current [30]. While the optical power is small, the tip of the electrical field vector evolves in the complex plane similarly to a 2-dimensional Brownian motion (2D-BM). In this situation the phase noise has an infinite variance with a statistics in the long time limit given by Cauchy's (or Lorentzian's) distribution [30]. The divergence of the phase variance means that numerical integration of this type of model can only give an approximation to the phase noise variance because the results depend on the chosen integration time step, no matter how small it is [30]. Since these results also hold when using the multiplicative noise models for a constant bias current below threshold, our aim in this work will be to analyze this constant current case from both, theoretical and experimental points of view.

In this paper we will first describe the additive and multiplicative noise rate equations models. The numerical solution of the gain-switched multiplicative noise model will be used to describe the conditions for which the additive and multiplicative noise models can be approximated by a 1-dimensional and 2D-BMs, respectively. Since the disparity of results lies mainly in the dimensionality of those motions we will analyze theoretically the problem by using the simplest equations for the 1-dimensional and 2D-BMs. The main statistical differences between the additive and multiplicative noise models will be illustrated and explained by using these simplified models. We will also obtain the time that takes the phase statistics in the multiplicative noise model to follow approximately Cauchy's distribution. In this way we will quantify when the condition of long-time limit [30] is reached.

In order to discern between the additive and multiplicative noise models we will measure the phase noise with a phase-diversity coherent receiver using a 90° optical hybrid. We will focus only on the case of a constant bias current below threshold since in that case the previous theoretical analysis has unveiled significant differences. We will develop a novel method to extract the phase noise directly from our measurements, that in contrast to the usual direct method [4], is not based on the analysis of the phase noise difference. The method permits a direct visualization of the phase noise trajectories that is accurate in the short time limit. Statistical moments of the phase noise are obtained by averaging over different phase noise trajectories. The obtained results are in very good agreement with the results obtained with the method based on the phase noise difference [4]. Our results show that the variance of the phase noise grows linearly in time and has Gaussian statistics, supporting the modelization of the phase noise statistics with the additive noise model. Our measurements also show that there is a dependence of the slope of the relation phase variance versus time on the frequency detuning between the semiconductor laser and the tunable laser of the coherent receiver. We find that there is a frequency detuning range around zero for which that slope is approximately constant, permitting us then to measure the diffusion coefficient of the phase noise.

The paper is organized as follows. We start with a description of the laser rate equations models. In section 3 we solve numerically the rate equations and discuss the Brownian motion approaches. Sections 4 and 5 are devoted to the theoretical analysis of 1-dimensional and 2D-BM, respectively. In section 6 the experimental method and results are presented. Finally, in section 7 we discuss our results and present our conclusions.

2. Semiconductor laser rate equations

In this section we detail the sets of rate equations that are typically used to describe the dynamics of the light emitted by semiconductor lasers. These are Ito's stochastic differential equations (SDE) with various degrees of complexity. The first SDE consider noise terms that have been derived from first principles for a system where the matter and the radiation have reached equilibrium [26]. These equations read [1, 24, 25, 33]

$$\frac{dP}{dt} = \left[\frac{G_N(N - N_t)}{1 + \epsilon P} - \frac{1}{\tau_p} \right] P + \beta B N^2 + \sqrt{2\beta B \bar{P} \bar{N}} F_p(t) \quad (1)$$

$$\frac{d\phi}{dt} = \frac{\alpha}{2} \left[G_N(N - N_t) - \frac{1}{\tau_p} \right] + \sqrt{\frac{\beta B}{2\bar{P}}} \bar{N} F_\phi(t) \quad (2)$$

$$\frac{dN}{dt} = \frac{I}{e} - (AN + BN^2 + CN^3) - \frac{G_N(N - N_t)P}{1 + \epsilon P} \quad (3)$$

where $P(t)$ is the photon number inside the laser, $\phi(t)$ is the optical phase in the reference frame corresponding to the resonant frequency at the threshold [33], and $N(t)$ is the number of carriers in the active region. The parameters appearing in the equations are the following: G_N is the differential gain, N_t is the carrier number at transparency, ϵ is the non-linear gain coefficient, τ_p is the photon lifetime, β is the fraction of spontaneous emission coupled into the lasing mode, α is the linewidth enhancement factor, I is the injected current, e is the electron charge, and A , B and C are the non-radiative, spontaneous, and Auger recombination coefficients, respectively. The Langevin terms $F_p(t)$ and $F_\phi(t)$ in equations (1) and (2), represent fluctuations due to spontaneous emission. They are taken as Gaussian variables with zero average, $\langle F_i(t) \rangle = 0$, and with the following correlation properties, $\langle F_i(t) F_j(t') \rangle = \delta_{ij} \delta(t - t')$, where $\delta(t)$ is Dirac's delta function and δ_{ij} the Kronecker delta function with the subindexes i and j referring to the variables P and ϕ . Two important points must be highlighted. First, i) the bias current I has a constant value, and ii) the constant steady-state average values of the variables, \bar{P} and \bar{N} , corresponding to I appear multiplying the Langevin terms, $F_p(t)$ and $F_\phi(t)$, that is why we term equations (1)–(3) as the additive noise model. When the steady-state has been reached ϕ diffuses in such a way that it has a Gaussian distribution with a variance, σ_ϕ^2 , that increases linearly with t , $\sigma_\phi^2 = 2D_\phi t$, where D_ϕ is the diffusion coefficient, given by [1, 23, 24]

$$D_\phi = \frac{\beta B \bar{N}^2}{4\bar{P}} \text{ if } I < I_{\text{th}}, \text{ and } D_\phi = \frac{\beta B N_{\text{th}}^2}{4\bar{P}} (1 + \alpha^2) \text{ if } I > I_{\text{th}} \quad (4)$$

where N_{th} is the carrier number at threshold given by $N_{\text{th}} = N_t + 1/(G_N \tau_p)$ and I_{th} is the threshold current.

In many applications semiconductor lasers are used in pulsed mode. The modulation of the bias current, that is $I = I(t)$, is a simple method to obtain those pulses. In particular, gain-switched laser pulses are obtained when the bias current goes from a below-threshold to an above threshold value. No semiconductor laser rate equations have been derived from first principles when $I = I(t)$. The procedure for describing laser dynamics in this case is the substitution of the averages in equations (1) and (2) by their corresponding variables. The considered equations are then [9, 16, 21, 22, 27–30, 34]:

$$\frac{dP}{dt} = \left[\frac{G_N(N - N_t)}{1 + \epsilon P} - \frac{1}{\tau_p} \right] P + \beta B N^2 + \sqrt{2\beta B P N} F_p(t) \quad (5)$$

$$\frac{d\Phi}{dt} = \frac{\alpha}{2} \left[G_N(N - N_t) - \frac{1}{\tau_p} \right] + \sqrt{\frac{\beta B}{2P}} N F_\phi(t) \quad (6)$$

$$\frac{dN}{dt} = \frac{I(t)}{e} - (AN + BN^2 + CN^3) - \frac{G_N(N - N_t)P}{1 + \epsilon P}. \quad (7)$$

In these equations P and Φ are the photon number and optical phase, respectively. In the equations for P and Φ the noise terms are multiplied by functions of the variables, P and N , that is why we term equations (5)–(7) as the multiplicative noise model. We distinguish the optical phase obtained from equation (6), Φ , to that obtained from equation (2), ϕ , because their evolution equations are different. In fact, when the injected current is below its threshold value the statistics of ϕ at the steady-state is Gaussian [1,

[24, 25, 33] while the corresponding statistics of Φ in the long-time limit is given by Cauchy's distribution [30]. The analysis in [30] was performed by using the equations for the complex electrical field, $E(t)$, that are equivalent to equations (5)–(7). These equations are [30]:

$$\frac{dE}{dt} = \left[\left(\frac{1}{1 + \epsilon |E|^2} + i\alpha \right) G_N(N - N_t) - \frac{1 + i\alpha}{\tau_p} \right] \frac{E}{2} + \sqrt{\frac{\beta B}{2}} N \xi(t) \quad (8)$$

$$\frac{dN}{dt} = \frac{I(t)}{e} - (AN + BN^2 + CN^3) - \frac{G_N(N - N_t) |E|^2}{1 + \epsilon |E|^2} \quad (9)$$

where $E(t) = E_1(t) + iE_2(t)$ is the complex electric field, $P(t) = |E|^2 = E_1^2 + E_2^2$, $\Phi(t) = \arctan(E_2/E_1)$, and $\xi(t) = \xi_1(t) + i\xi_2(t)$ is the complex Gaussian white noise with zero average and correlation given by $\langle \xi(t)\xi^*(t') \rangle = 2\delta(t - t')$ that represents the spontaneous emission noise. These equations can be integrated to find Φ with no numerical instabilities, in contrast to equations (5)–(7) in which the integration is unstable when the current is below threshold due to the presence of $P^{1/2}$ and $P^{-1/2}$ in the terms multiplying the noise terms [30]. As mentioned above the statistical properties of Φ are very different to those of ϕ when the current is below threshold. In fact, due to Cauchy's distribution of Φ the variance of Φ diverges [30], that is $\sigma_\Phi^2 = \infty$, while the variance of ϕ , σ_ϕ^2 , remains finite. In other words, no convergence of the value of σ_Φ is found when the integration time step is decreased, even to tiny values. The difference between the values of σ_ϕ and σ_Φ lies on the dimensionality of the Brownian motion that the variables are displaying, as we will detail in the next sections. The evolution of ϕ can be well approximated by a 1D-BM in equation (2) when $I < I_{th}$ because the noise term dominates over the deterministic term. In this way the distribution of ϕ is Gaussian and finite values of σ_ϕ^2 are obtained with the linear dependence on t characteristic of the 1-dimensional diffusion process. The situation is different for Φ . For bias currents below threshold the evolution of $E(t)$ in the complex plane can be approximated by a 2D-BM. This is the main reason of the previously mentioned results: σ_Φ^2 is infinite because the variance of the polar angle in 2D-BM is infinite [35], and the statistical distribution of Φ in the long time limit tends to Cauchy's distribution because that is the theoretical result obtained for the polar angle in 2D-BM [36].

3. Numerical analysis of the rate equations: the Brownian motion approach

In this section we first solve numerically equations (8) and (9) in the pulsed regime to illustrate the approximation of the dynamics of the variables using Brownian motion. We show in figure 1 the dynamical evolution of P , Φ , N , and of the frequency chirp. Since Φ is the optical phase with respect to that corresponding to the resonant frequency at the threshold current, ν_{th} , the electrical field is written as

$$E(t) = E_1(t) + iE_2(t) = \sqrt{P(t)} e^{i(2\pi\nu_{th}t + \Phi(t))} \quad (10)$$

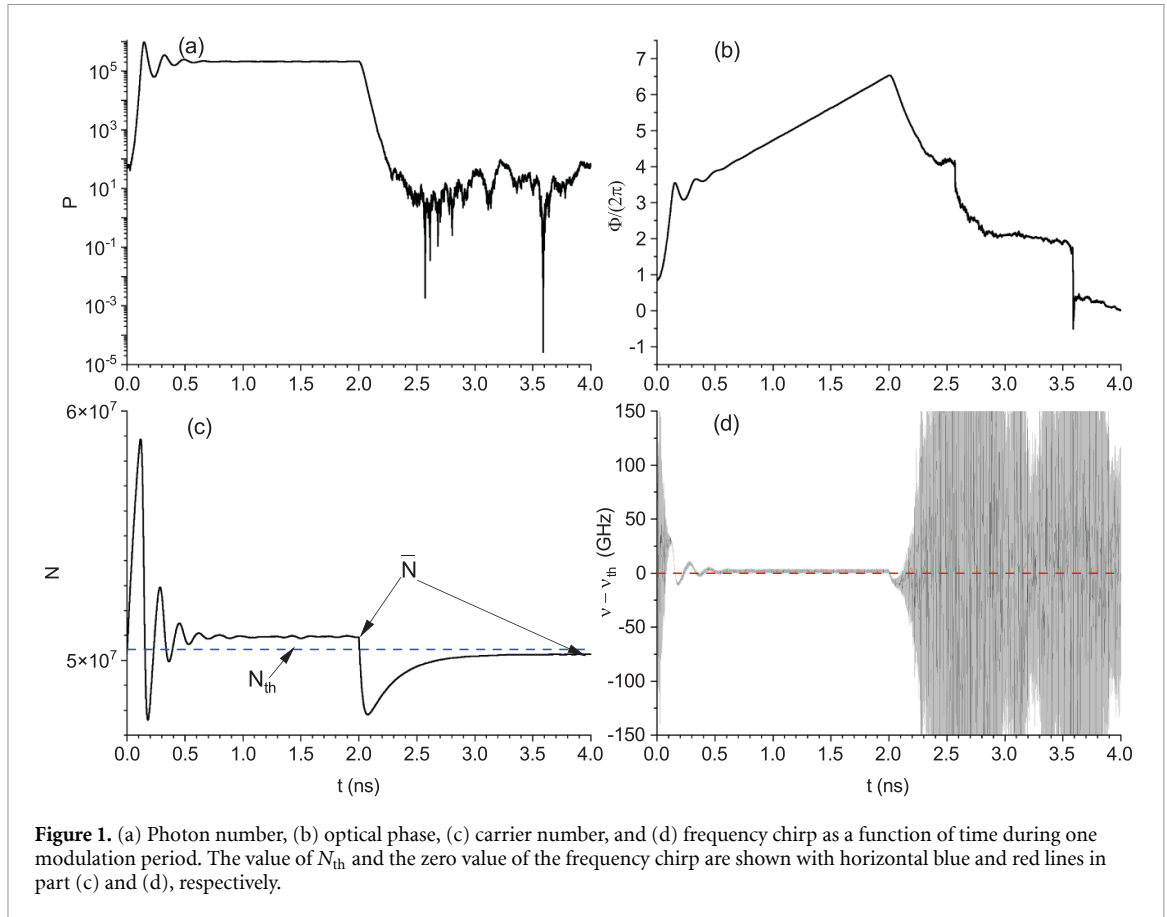
the instantaneous optical frequency is given by

$$\nu(t) = \nu_{th} + \frac{1}{2\pi} \frac{d\Phi}{dt} \quad (11)$$

and the frequency chirp is defined as $\frac{1}{2\pi} \frac{d\Phi}{dt} = \nu - \nu_{th}$.

Numerical integration has been performed by using the Euler–Maruyama algorithm [37, 38] with an integration time step of $\Delta t = 0.01$ ps. We have chosen the following values of the parameters: $G_N = 1.48 \times 10^4 \text{ s}^{-1}$, $N_t = 1.93 \times 10^7$, $\epsilon = 7.73 \times 10^{-8}$, $\tau_p = 2.17$ ps, $\alpha = 3$, $\beta = 5.3 \times 10^{-6}$, $A = 2.8 \times 10^8 \text{ s}^{-1}$, $B = 9.8 \text{ s}^{-1}$, and $C = 3.84 \times 10^{-7} \text{ s}^{-1}$. These parameters correspond to the extracted parameters of a single longitudinal mode discrete mode laser with a threshold current of $I_{th} = 14.14$ mA at 25 °C [29, 34]. We consider that $I(t)$ follows a square-wave modulation of period T with $I(t) = I_{on}$ during $T/2$, and $I(t) = I_{off}$ during the rest of the period. We take $I_{on} = 30$ mA, $T = 4$ ns, and a switch-off current below threshold, $I_{off} = 14$ mA.

Figure 1(a) shows that the optical pulse builds up from very small noisy values at short values of t . Typical relaxation oscillations are observed in figures 1(a) and (c) until the system reaches the steady-state corresponding to I_{on} at around 1 ns. For $t > 2$ ns the current changes to a value below I_{th} and both P and N decrease until P reaches the levels in which spontaneous emission dominates the evolution. Figure 1(c) shows that N recovers up to the constant value corresponding to the steady-state, \bar{N} . The value of \bar{N} depends on the current I in such a way that is below (above) N_{th} if $I < I_{th}$ (if $I > I_{th}$) (see figure 1(c) where \bar{N} and N_{th} are indicated). Analytical expressions of \bar{N} can be found for $I < I_{th}$ [23] and for $I > I_{th}$ [39]. Figures 1(b) and



(d) also show relaxation oscillations in the initial stages of the evolution of the phase and frequency chirping. Oscillations in the chirping are directly related to the oscillations in N because equation (6) can be rewritten, using equation (11), as

$$\nu - \nu_{th} = \frac{\alpha G_N (N - N_{th})}{4\pi} + \frac{1}{2\pi} \sqrt{\frac{\beta B}{2P}} N F_\phi(t). \quad (12)$$

Figure 1(d) shows that at short times ($t < 0.1$ ns) the chirping has strong fluctuations because P is small and so the noise term is much larger than the deterministic term in equation (12). As t increases, the laser is in a transient regime where P and N oscillate with large values of P (see figures 1(a) and (c) for 0.1 ns $< t < 0.6$ ns). In this situation the noise term in equation (12) is smaller than the deterministic term, the frequency chirp is mainly deterministic and so it is directly proportional to N . As time increases, N begins to reach its steady state value, \bar{N} , and the deterministic term in equation (12) becomes $\frac{\alpha G_N (\bar{N} - N_{th})}{4\pi}$. This term is called the adiabatic chirp. In this time region the deterministic term is slightly larger than the noise term. From data in figure 1(d) we calculate the averaged and standard deviation of $\nu - \nu_{th}$ in the interval (1.7, 2) ns: their values are 1.85 GHz and 0.62 GHz, respectively. This average value can be easily estimated because $\frac{\alpha G_N (\bar{N} - N_{th})}{4\pi} \approx \frac{\alpha \epsilon (I_{on} - I_{th})}{4\pi e}$ [39], that for our parameters is 1.83 GHz. In the time region in which the frequency chirp is dominated by the adiabatic chirp the optical phase increases linearly with t (see figure 1(b) for $t < 2$ ns) with a slope given by $\frac{\alpha \epsilon (I_{on} - I_{th})}{2e}$.

The most interesting evolution region appears when $t > 2$ ns because most of the phase randomization occurs there. The deterministic part of the frequency chirping, $\frac{\alpha G_N (N - N_{th})}{4\pi}$, becomes negative because $N < N_{th}$ (see figure 1(c)), causing an initial deterministic decrease of Φ that can be seen in figure 1(b). Fluctuations of Φ become important when P reaches small values ($t > 2.3$ ns) that makes the frequency chirping being dominated by the noise term (see also figure 1(d)). When t increases in such a way that the steady-state is approached this deterministic part tends to $\frac{\alpha G_N (\bar{N} - N_{th})}{4\pi}$ that is -0.67 GHz for our parameters. This value is much smaller than the noise term in equation (12), as it can be seen in figure 1(d): when 3 ns $< t < 4$ ns, $\nu - \nu_{th}$ fluctuates with amplitudes much larger than the deterministic chirp (they can go up to several hundred GHz). Therefore in the time region where N is close to its steady-state value, equation (12)

can be approximated by

$$\nu - \nu_{\text{th}} = \frac{1}{2\pi} \sqrt{\frac{\beta B}{2P}} \bar{N} F_{\phi}(t). \quad (13)$$

Written in terms of Φ this equation is

$$\frac{d\Phi}{dt} = \sqrt{\frac{\beta B}{2P}} \bar{N} F_{\phi}(t) \quad (14)$$

that leads to an equation for the electrical field given by

$$\frac{dE}{dt} = \sqrt{\frac{\beta B}{2}} \bar{N} \xi(t) \quad (15)$$

that corresponds to a 2D-BM in the (E_1, E_2) plane.

If our departure equations were equations (1)–(3) instead equations (8) and (9) we get that

$$\frac{d\phi}{dt} = \sqrt{\frac{\beta B}{2P}} \bar{N} F_{\phi}(t) \quad (16)$$

would describe the evolution in a similar regime to that considered for obtaining equation (15). In this regime ϕ is describing a 1D-BM. The difference in the evolution equations for ϕ and Φ is that P is averaged in equation (16) while it is not in equation (14). This difference will be essential for determining the statistical differences between ϕ and Φ . The equations describing 1D-BM and 2D-BM will be solved numerically in the following sections to highlight their main differences. We will restrict to situations in which the injected current is constant and below threshold. In this way the equations describing 1D-BM, equation (16), and 2D-BM, equation (15), have constant diffusion coefficients. Also, in order to simplify our analysis as much as possible, we will consider the dimensionless 1D-BM and 2D-BM with diffusion coefficients equal to one.

4. Analysis of the 1D-BM

The stochastic process $X(t)$ known as 1D-BM satisfies the following Langevin equation

$$\frac{dx}{dt} = \sqrt{2D} \xi(t) \quad (17)$$

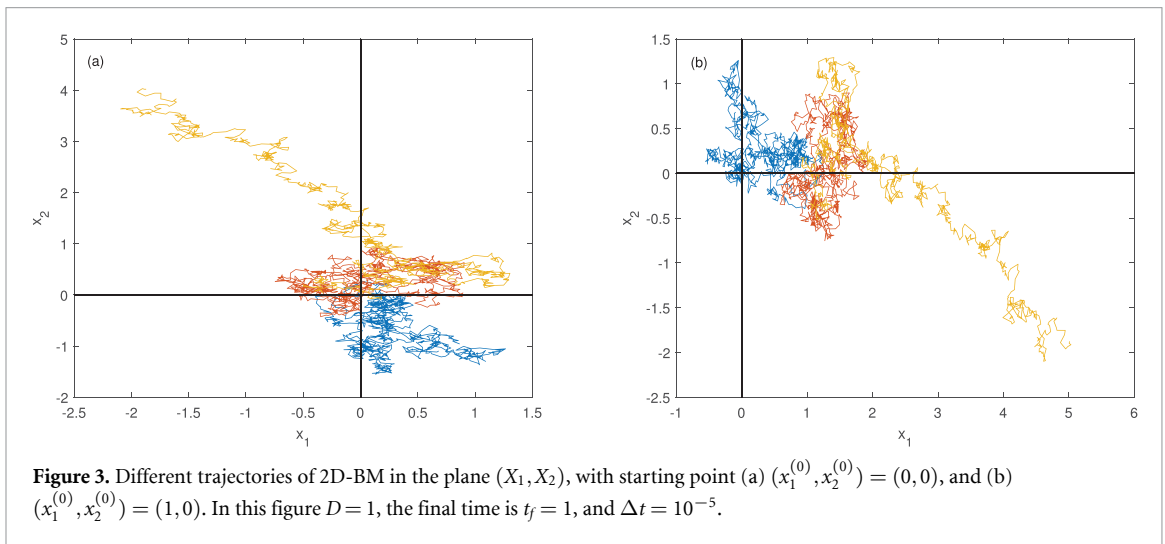
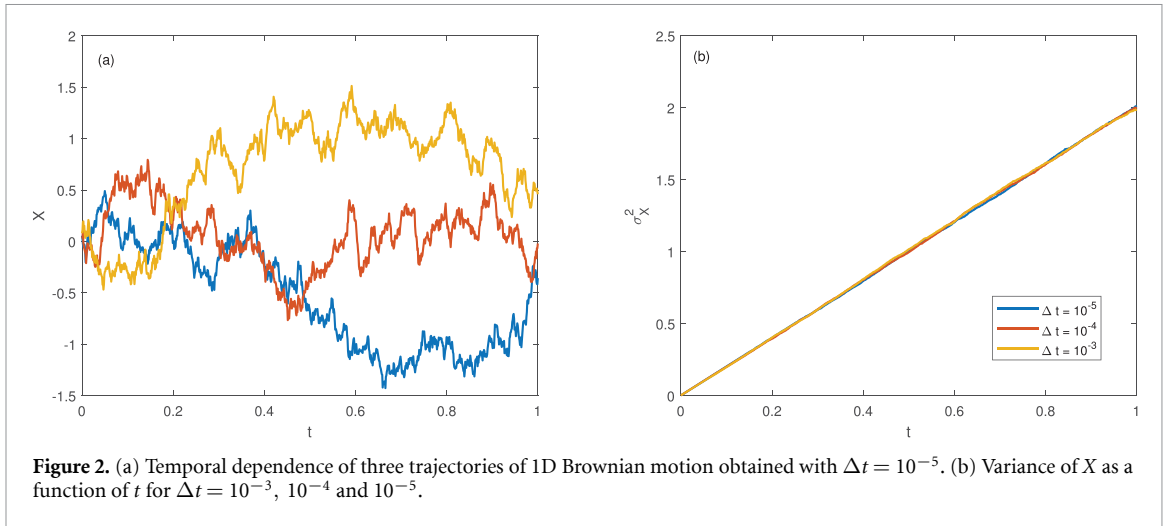
where $-\infty < x < \infty$, D is the diffusion coefficient and $\xi(t)$ is a real Gaussian white noise with $\langle \xi(t) \rangle = 0$, and $\langle \xi(t) \xi(t') \rangle = \delta(t - t')$. This equation can be solved analytically for $X(0) = x_0$ to obtain that $X(t)$ has Gaussian statistics with $\langle X(t) \rangle = x_0$ and a variance, $\sigma_X^2(t) = 2Dt$ [40].

We now solve numerically this equation by using the Euler–Maruyama algorithm with $D = 1$ and $x_0 = 0$ in order to illustrate the shape of the obtained trajectories. Figure 2(a) shows three different trajectories obtained with an integration time step of $\Delta t = 10^{-5}$. In order to obtain results statistically significant we generate $N = 10^4$ different trajectories to calculate averages as a function of time. The mean value (not shown) is very close to zero and the variance grows linearly with t with a slope of 2 as it can be seen in figure 2(b). In this figure we also include the results obtained with different Δt in order to check the convergence of the numerical integration method. Figure 2(b) shows how the variance converges to the theoretical line $\sigma_X^2(t) = 2Dt$ when reducing Δt . In fact even the results obtained with the largest value of $\Delta t = 10^{-3}$ show good agreement with the theoretical result. We have also checked that the distribution of $X(t)$ gradually changes from Dirac's delta at $t = 0$, towards a Gaussian as t increases. We have checked (not shown) that the distribution at $t = 1$ closely follows the theoretical Gaussian shape. The application of these results to the optical phase, that is, $X(t) = \phi(t)$, gives some of the initial expressions. For instance, the comparison of equations (16) and (17) gives the expression of the phase diffusion coefficient when $I < I_{\text{th}}$ in equation (4).

5. Analysis of the 2D-BM

The 2D-BM is defined by two stochastic processes, $X_1(t)$ and $X_2(t)$, that satisfy the Langevin equations

$$\frac{dx_i}{dt} = \sqrt{2D} \xi_i(t) \quad (18)$$



where $-\infty < x_i < \infty$, D is the diffusion coefficient, $\xi_1(t)$ and $\xi_2(t)$ are real Gaussian white noises, statistically independent one from the other, with $\langle \xi_i(t) \rangle = 0$, $\langle \xi_i(t)\xi_j(t') \rangle = \delta(t-t')\delta_{ij}$, and $i, j = 1, 2$. The starting point is $(X_1(0), X_2(0)) = (x_1^{(0)}, x_2^{(0)})$.

As the two variables X_1 and X_2 are independent, and both follow the 1D-BM equations, analysing them separately will give the exact same results already discussed in the previous section. However, the study of the trajectories in polar coordinates, that is in terms of a radius $a(t)$ and an angle or phase $\Phi = \Phi(t)$, gives novel results with respect to the 1-dimensional case. These variables are written in terms of $X_i(t)$ as $P(t) = a^2(t) = X_1^2 + X_2^2$, and $\Phi(t) = \arctan(X_2/X_1)$.

Figures 3(a) and (b) show the numerical solution of equation (18) with $D = 1$ for two different initial conditions $(x_1^{(0)}, x_2^{(0)}) = (0, 0)$, and $(1, 0)$, respectively. Three different trajectories, obtained with an integration time step of $\Delta t = 10^{-5}$, are shown for each figure. The trajectories are shown in the (X_1, X_2) plane. The highly irregular trajectories, typical of Brownian motion, will be discussed in relation to figures 4(a) and 5(a) in which the corresponding temporal evolution of the optical phase will be shown. This phase is a continuous and unbounded quantity that can be calculated from $\Phi(t) = \arctan(X_2/X_1)$. Since this function only takes values in the interval $[-\pi/2, \pi/2]$, it is important to count how many times the trajectory crosses the vertical axis $X_1 = 0$ to obtain a continuous and unbounded phase. We have used the algorithm described in appendix B of [30] to calculate $\Phi(t)$. Figure 4(a) shows the values of $\Phi(t)$ for the trajectories shown in figure 3(a). At a first look, $\Phi(t)$ could resemble the phase for 1D-BM trajectories shown in figure 2. However a better comparison can be made if statistical moments of Φ are calculated. We generate numerically 10^4 trajectories to calculate those moments. The average of $\Phi(t)$ (not shown) is very close to zero, similarly to the 1D-BM case. However the dynamical evolutions of the variance in 1D-BM and 2D-BM are very different. Figure 4(b) shows the variance of $\Phi(t)$, σ_Φ^2 , for three different integration steps. Two main points can be

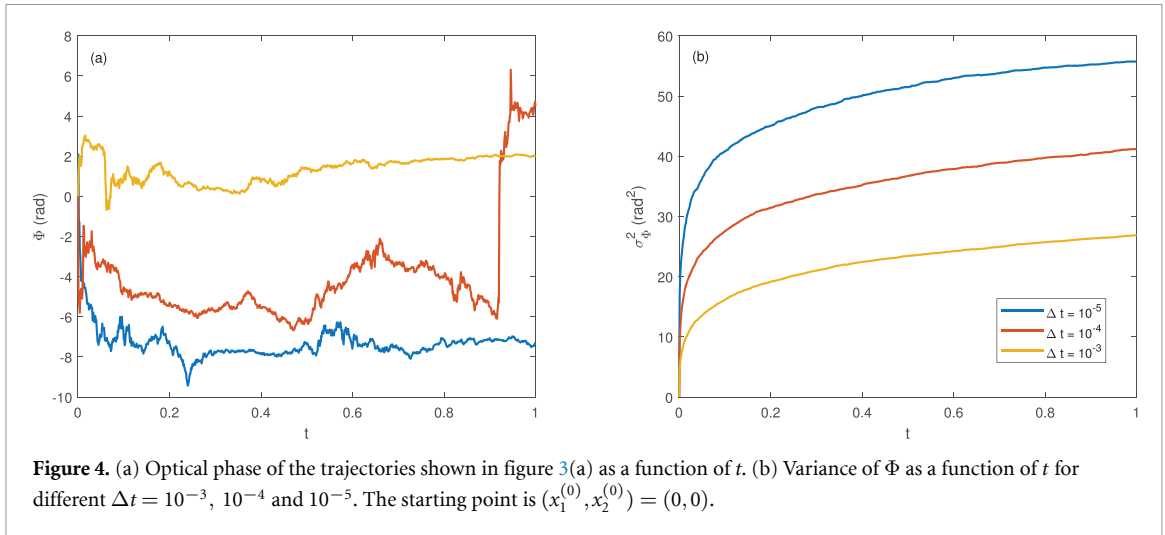


Figure 4. (a) Optical phase of the trajectories shown in figure 3(a) as a function of t . (b) Variance of Φ as a function of t for different $\Delta t = 10^{-3}$, 10^{-4} and 10^{-5} . The starting point is $(x_1^{(0)}, x_2^{(0)}) = (0, 0)$.

highlighted. First, σ_{Φ}^2 is no longer a linear function of t , in contrast to the linearity observed in figure 2(b). Second, σ_{Φ}^2 does not converge as Δt decreases, in contrast to the convergence observed in figure 2(b).

The analysis of individual trajectories in figure 4(a) show that Φ changes very fast at initial times, increasing or decreasing to certain positive or negative value. Then, it can stabilise for a long period of time like in the yellow and blue trajectories (see figures 4(a) and 3(a)). Later on, the trajectory might change abruptly again, like in the red trajectory of figure 4(a). This occurs since the starting point is the origin (0,0) and at the beginning the trajectories can move around the quadrants with very small steps, making the phase vary abruptly. Later, it is reasonable to think that the trajectory will displace from (0,0) to one of the quadrants, thus making it more difficult for Φ to change so abruptly. In the case that (X_1, X_2) for any chance come back close to the origin again, like the red trajectory does, (see figure 3(a)) these abrupt changes can occur again as shown in figure 4(a) for $t \sim 0.9$.

The reason why no convergence of σ_{Φ}^2 is obtained in figure 4(b) as Δt decreases is that $\sigma_{\Phi}^2 = \infty$. This occurs since X_1 and X_2 are independent Gaussian random variables. From these variables the distribution of P can be calculated: $P(t)$ is an exponential random variable, with a probability density $f(P)$ given by $f(P) = \frac{e^{-\frac{P}{\langle P \rangle}}}{\langle P \rangle}$ if $P \geq 0$, and 0 if $P < 0$. The mean value of P can be calculated as follows: $\langle P \rangle = \langle X_1^2 \rangle + \langle X_2^2 \rangle = \sigma_{X_1}^2 + \langle X_1 \rangle^2 + \sigma_{X_2}^2 + \langle X_2 \rangle^2 = 2Dt + (x_1^{(0)})^2 + 2Dt + (x_2^{(0)})^2$, so $\langle P(t) \rangle = P(0) + 4Dt$. The Langevin equation that describes $\Phi(t)$ is $\frac{d\Phi}{dt} = \sqrt{\frac{2D}{P}} F_{\Phi}(t)$, where $F_{\Phi}(t)$ is a real Gaussian white noise such that $\langle F_{\Phi}(t) \rangle = 0$, and $\langle F_{\Phi}(t) F_{\Phi}(t') \rangle = \delta(t - t')$ [30]. $\sigma_{\Phi}^2 = \infty$ since the variance of the phase is $\sigma_{\Phi}^2 = 2D \langle 1/P \rangle t$, and $\langle 1/P \rangle = \int_0^{\infty} \frac{1}{P} \frac{e^{-\frac{P}{\langle P \rangle}}}{\langle P \rangle} dP = \infty$ [30].

Figure 4(b) shows that for small times, the variance increases almost vertically. This is because as said before, (0, 0) is a singular point, and when trajectories are close to it they might vary really fast and $\sigma_{\Phi}^2 \propto \langle 1/P \rangle$. Near (0, 0) P is almost 0, and $1/P$ tends to infinity. When P increases, i.e. the square of the distance to the origin increases, $1/P$ is smaller and the variance of the phase σ_{Φ}^2 will increase slower. This perfectly summarizes this idea that getting closer to (0, 0) involves faster variability in Φ , and getting away from it means the trajectory is deep into some quadrant, with high P and low phase variability.

To further analyse 2D-BM, it seems reasonable to study processes with a starting point further away from the origin. Thus, the rapid increase of the variance for smaller times should be avoided. That is why the case $(x_1^{(0)}, x_2^{(0)}) = (1, 0)$ is studied next, which also has a starting phase $\Phi = 0$ and hence the mean $\langle \Phi \rangle$ is also zero. Three trajectories are shown in figure 3(b) and their respective phases in figure 5(a). The first result to notice is how now the phase does not abruptly change at initial times, as was expected. The variance of the phase σ_{Φ}^2 over time is also shown in figure 5(b). The variance does not increase faster for small times than longer times. Moreover, as seen before, when Δt is reduced, the variance always increases, showing that the divergence of σ_{Φ}^2 appears independently of the initial condition, as was shown theoretically in [35]. Also σ_{Φ}^2 is not a linear function of time like in 1D-BM. This is once again because $\sigma_{\Phi}^2 \propto \langle 1/P \rangle$, which is not constant since P is a time-dependent random variable. As an illustration of the time dependence of the statistics of P we show in figure 6(a) the mean value of P over time when $\Delta t = 10^{-3}$, 10^{-4} and 10^{-5} . The plot shows how $\langle P(t) \rangle = P(0) + 4Dt$ is fulfilled. In this case $P(0) = (x_1^{(0)})^2 + (x_2^{(0)})^2 = 1$ and since $D = 1$, the slope of the line is 4. Similar results are obtained for all Δt , showing that P , contrary to Φ , has finite

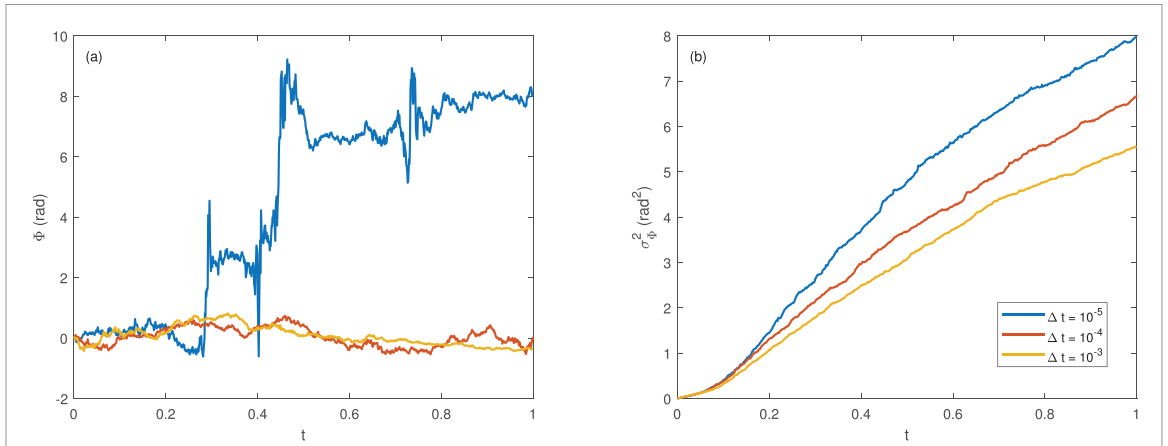


Figure 5. (a) Optical phase of the trajectories shown in figure 3(a) as a function of t . (b) Variance of Φ as a function of t for different $\Delta t = 10^{-3}, 10^{-4}$ and 10^{-5} . The starting point is $(x_1^{(0)}, x_2^{(0)}) = (1, 0)$.

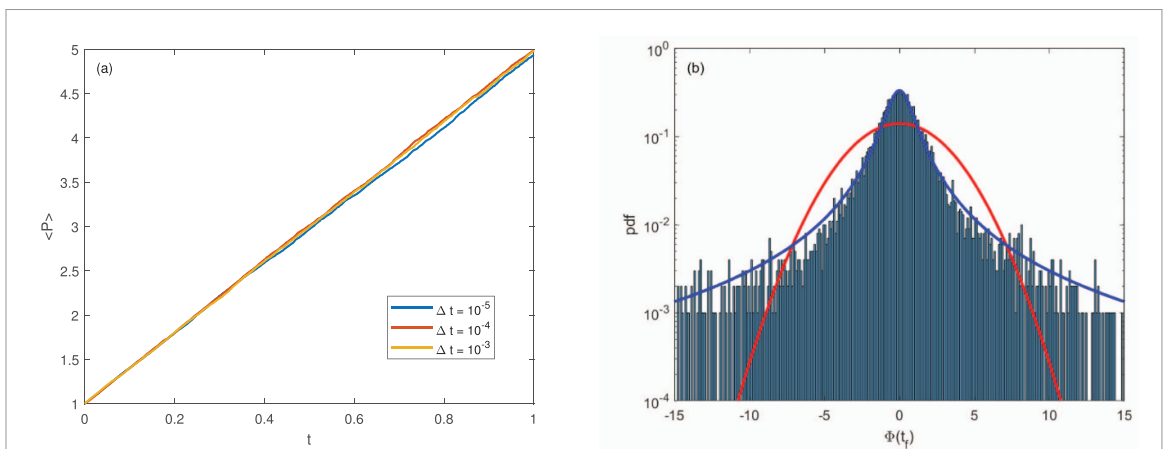


Figure 6. (a) Mean of P over time t for different $\Delta t = 10^{-3}, 10^{-4}$ and 10^{-5} . (b) pdf of $\Phi(t_f)$ of a 2D-BM for $t_f = 1, D = 1, (x_1^{(0)}, x_2^{(0)}) = (0, 0)$, and $\Delta t = 10^{-5}$. Theoretical values of Cauchy (blue line) that best fit the numerical data, and Gaussian (red line) distribution with a standard deviation given by the standard deviation of the data.

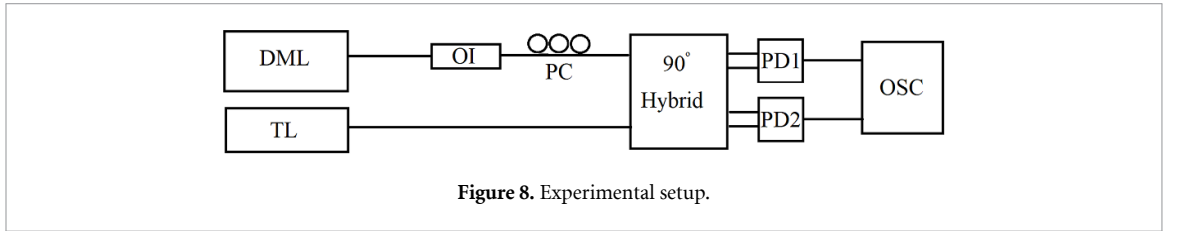
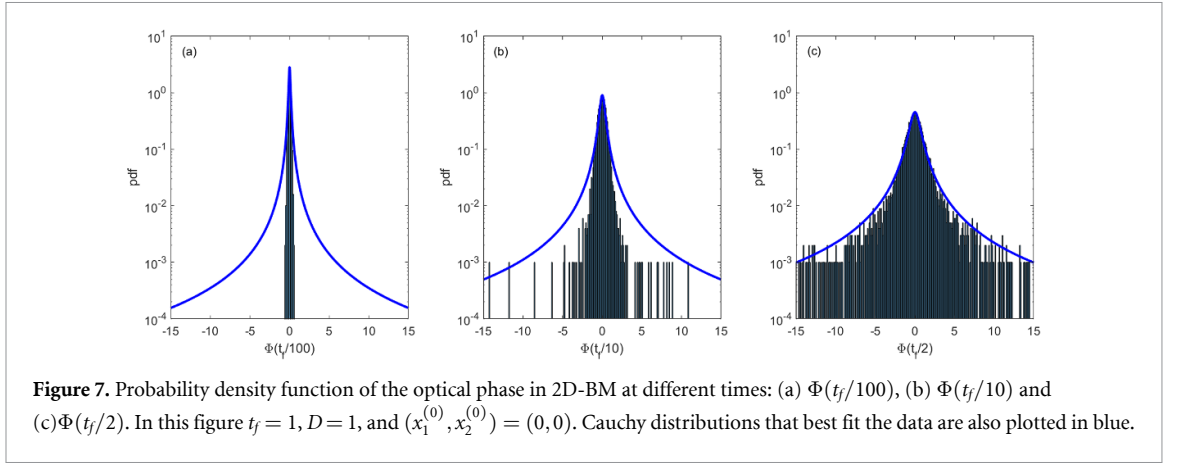
moments, which do converge when Δt is decreased. This happens because P is described by an exponential distribution, as shown previously.

It is also insightful to study the probability density function (pdf) of the phase at the last integration time, $\Phi(t_f)$. This is shown in figure 6(b), using a vertical logarithmic scale for visualising better the tails of the distribution. The plot also shows Cauchy (also known as Lorentzian) pdf with mean value 0 and γ parameter:

$$f(\Phi) = \frac{1}{\pi \gamma} \frac{1}{1 + \left(\frac{\Phi}{\gamma}\right)^2}. \tag{19}$$

We have chosen the γ value for which the best fit of the numerical results is obtained. Cauchy’s probability approximates the data closely, also on the tails of the distribution. We have also plotted the Gaussian distribution with the standard deviation of the data. Figure 6(b) shows that the Gaussian pdf fails to describe the distribution of the numerical data.

These results are in agreement with Spitzer’s theorem [36] that shows that Φ tends to a Cauchy distribution for $t \rightarrow \infty$, showing that a good approximation to that distribution is already obtained at $t = 1$. Therefore, it is insightful to analyse the distribution of Φ also at intermediate times, to try to visualise its evolution in time. It is clear that at $t = 0$ the distribution is Dirac’s delta, since all trajectories start at $\Phi(0) = 0$. But with time, trajectories start to spread, going away from zero. In figure 7 the distributions for $t = t_f/100, t = t_f/10$ and $t = t_f/2$ are plotted. The results in figure 7 show that the distribution of trajectories approaches Cauchy distribution very quickly in time. For $t = t_f/100 \equiv 0.01$ and $t = t_f/10 \equiv 0.1$, the distribution is already close in the center, but is quite far in the tails. For a time $t = t_f/2 \equiv 0.5$, the distribution already approximates the data closely, in the centre and the tails, just like what happens for



$t = t_f \equiv 1$. This shows that $t \rightarrow \infty$, in the sense of Spitzer's theorem, in this case is already achieved for times greater than $t = 0.5$.

6. Experimental analysis of the optical phase

The experimental setup is shown in figure 8. A single polarization 90° optical hybrid (kylia COH24) is used to measure the phase from a single longitudinal mode discrete mode laser (DML) described in [29, 34]. The bias current and the temperature of the laser were controlled with a laser driver and a temperature controller (Luzwavelabs LDC/E-Current200 and LDC/E-Temp3), respectively. The temperature and the current of the device were held constant at 25°C and 14 mA , respectively. This value of the current is below the threshold current, $I_{\text{th}} = 14.14\text{ mA}$, measured at that temperature. The optical wavelength measured at 14 mA is $\lambda_s = 1546.864\text{ nm}$. The light emitted by the DML passes through an optical isolator (OI) and a polarization controller (PC) entering into one of the inputs of the hybrid. The other input is fed with light from a tunable laser (TL) (Pure Photonics PPCL300) with a narrow linewidth (75 kHz) and a constant power of 4 mW . The outputs from the hybrid go to two balanced amplified photodetectors (PD1 and PD2, Thorlabs PDB480C-AC) with 1.6 GHz bandwidth that are connected to two channels of a real-time oscilloscope (OSC, Keysight DSO91204A, with 13 GHz bandwidth).

The electrical output at photodetectors 1 and 2, PD1 and PD2, are proportional to $\text{PD}_1(t) = \frac{1}{\sqrt{2}}A_s A_{\text{TL}} \sin[(\omega_s - \omega_{\text{TL}})t + \varphi(t)]$, and $\text{PD}_2(t) = \frac{1}{\sqrt{2}}A_s A_{\text{TL}} \cos[(\omega_s - \omega_{\text{TL}})t + \varphi(t)]$, respectively. In these equations A_s is the amplitude of the signal (the electrical field corresponding to the DML is $S(t) = A_s \exp[i(\omega_s t + \varphi(t))]$), A_{TL} is the amplitude of the electrical field corresponding to the TL, $\text{TL}(t) = A_{\text{TL}} \exp[i\omega_{\text{TL}} t]$, ω_s and ω_{TL} are the angular optical frequencies of DML and TL, and $\varphi(t)$ is the phase noise of the DML, the quantity that we want to measure. In these equations we have also considered that the TL has phase noise much smaller than the DML, a condition that is clearly fulfilled for the values of the current that we apply to the DML, close to I_{th} .

We calculate the phase that appears in $\text{PD}_1(t)$ and $\text{PD}_2(t)$, $\theta(t)$, given by

$$\theta(t) = \Delta\omega t + \varphi(t), \quad (20)$$

where $\Delta\omega = \omega_s - \omega_{\text{TL}}$, from the values of the electrical signals at each photodetector by using the algorithm detailed in appendix B of [30]. $\theta(t)$ is an unbounded phase from which we can extract $\varphi(t)$ providing $\Delta\omega$ is calculated. We show in figure 9(a) the evolution of five trajectories obtained for a current of $I = 14\text{ mA}$, and 2 GSa/s sampling rate. The wavelength of the TL, λ_{TL} , is 1546.864 nm that is the value that maximizes the amplitude of the signals at the oscilloscope ($V_{\text{rms}} \sim 330\text{ mV}$). These trajectories are obtained from a long sequence of data (of 0.01 s duration) as follows. This sequence is divided in windows of duration $T_w = 1\mu\text{s}$.

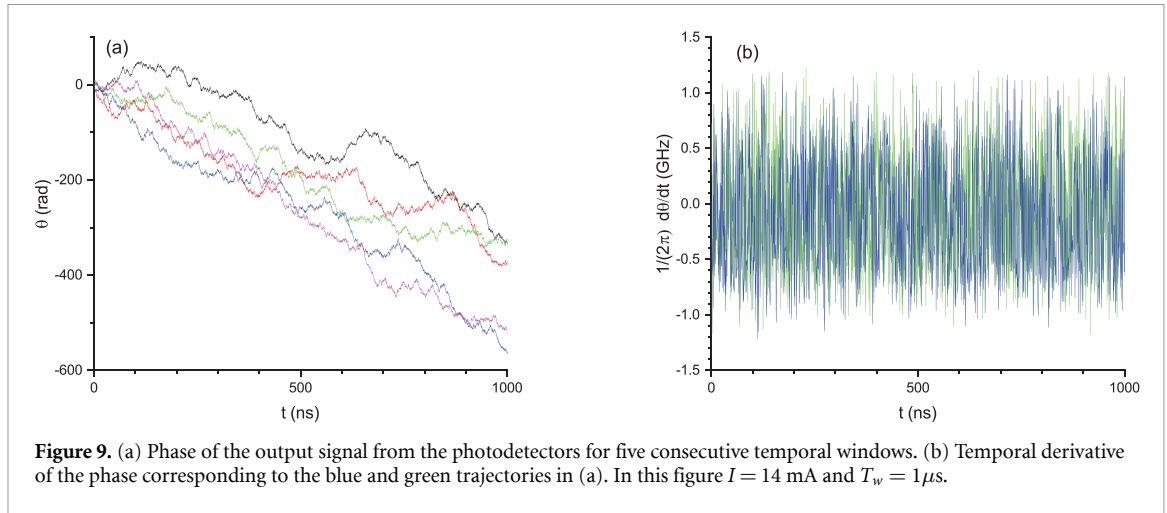


Figure 9. (a) Phase of the output signal from the photodetectors for five consecutive temporal windows. (b) Temporal derivative of the phase corresponding to the blue and green trajectories in (a). In this figure $I = 14$ mA and $T_w = 1 \mu\text{s}$.

Results corresponding to five consecutive windows are overlaid in this temporal window in such a way that the initial value, $\theta(0)$, is that corresponding to the end of the previous window but converted into the $[-\pi, \pi]$ interval. $\theta(t)$ fluctuates with a clear decreasing drift that corresponds to negative and small values of $\Delta\omega$.

Fluctuations of the instantaneous optical frequency of semiconductor lasers appear due to several causes like fluctuations in the internal temperature of the laser and $1/f$ noise [4]. Fluctuations of the instantaneous frequency on long time scales are large [41] so measurements in short time windows must be performed so that those instantaneous frequencies, and so $\Delta\omega$, can be considered as approximately constant in each window. The measurement of $\Delta\omega$ is performed for each temporal window in the following way. We derive equation (20) to obtain

$$\frac{d\theta}{dt} = \Delta\omega + \frac{d\varphi}{dt}. \quad (21)$$

Deriving the phase of the DML, $\omega_s t + \varphi(t)$, we obtain $\omega_s + \frac{d\varphi}{dt}$. The average of this quantity over different trajectories, $\omega_s + \langle \frac{d\varphi}{dt} \rangle$ must be the angular frequency of the DML, ω_s , and therefore $\langle \frac{d\varphi}{dt} \rangle = 0$. Applying this result in the average of equation (21) we obtain that

$$\Delta\omega = \langle \frac{d\theta}{dt} \rangle. \quad (22)$$

Since our bias current is constant, $\frac{d\theta}{dt}$ is a stationary stochastic process. This is illustrated in figure 9(b) in which the values of $\frac{1}{2\pi} \frac{d\theta}{dt}$ corresponding to the blue and green trajectories of figure 9(a) are plotted. Figure 9(b) shows that statistical properties of $\frac{d\theta}{dt}$ do not change with t , confirming the stationary character of the process. For this type of processes averages over different trajectories coincide with time averages, and therefore

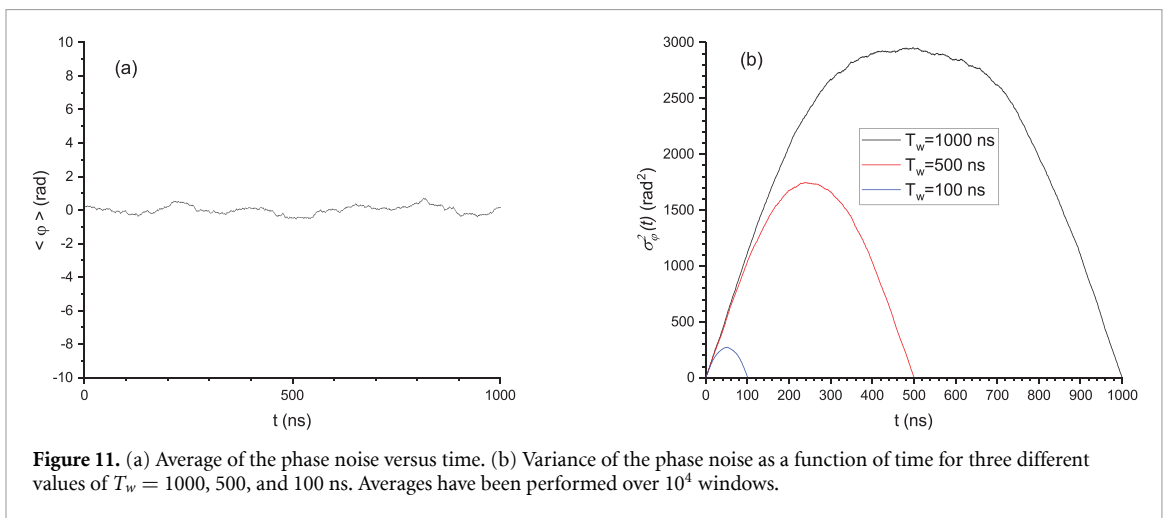
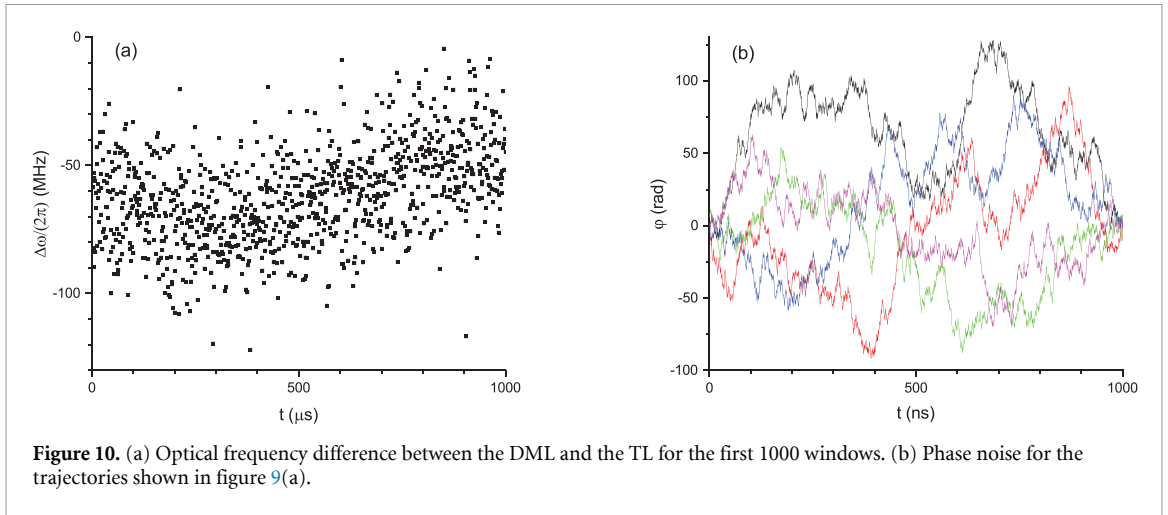
$$\Delta\omega = \overline{\frac{d\theta}{dt}} \quad (23)$$

where $\overline{\frac{d\theta}{dt}}$ is the temporal average of $\frac{d\theta}{dt}$ over a window of duration T_w . After calculating time averages in figure 9(b) over the $1 \mu\text{s}$ window, we obtain that $\Delta\omega/(2\pi)$ is -89.6 and -52.8 MHz for the blue and green trajectories, respectively. To better illustrate the fluctuations of these quantities we have plotted in figure 10(a) the values of $\Delta\omega/(2\pi)$ for the first 1000 windows contained in our long sequence. $\Delta\omega/(2\pi)$ fluctuates around its averaged value, $\langle \Delta\omega/(2\pi) \rangle = -62.2$ MHz, with a standard deviation of 18.6 MHz.

We can now plot the phase noise by using $\varphi(t) = \theta(t) - \Delta\omega t$. The results corresponding to the five realizations shown in figure 9(a) are plotted in figure 10(b). This figure shows the typical broadening of the trajectories during the initial stages of the window. However that broadening is not maintained because it is clear that the value of $\varphi(t)$ approaches zero at the end of the window, $\varphi(T_w) \sim 0$, for all the trajectories.

The previous result can be understood as follows. From equation (21) we obtain that $\frac{d\varphi}{dt} = \frac{d\theta}{dt} - \Delta\omega$. $\frac{d\varphi}{dt}$ is a stationary process (it is obtained from $\frac{d\theta}{dt}$ by subtracting a constant) so $\langle \frac{d\varphi}{dt} \rangle = \overline{\frac{d\varphi}{dt}}$. Since $\langle \frac{d\varphi}{dt} \rangle = 0$ we obtain that

$$\overline{\frac{d\varphi}{dt}} = 0 = \frac{1}{T_w} \int_0^{T_w} \frac{d\varphi}{dt} dt \quad (24)$$



where we have used the definition of temporal average over T_w . The value of $\varphi(T_w)$ in terms of $\frac{d\varphi}{dt}$ is $\varphi(T_w) = \int_0^{T_w} \frac{d\varphi}{dt} dt$ and using equation (24) we obtain that $\varphi(T_w) = 0$.

Let us now calculate the averages of the phase as done previously for the Brownian motion. We show in figure 11 the mean value and the variance of φ . The mean value is calculated by averaging over 10^4 windows of duration $T_w = 1000$ ns. As expected, the average is close to zero for all times. The variance is shown in figure 11(b) for three different values of T_w , being averaged also over 10^4 windows. The qualitative behavior of σ_φ^2 is similar in the three cases. After an initial linear increase, the variance reaches a maximum and then decreases until $\sigma_\varphi^2(T_w) = 0$ because, as previously explained, $\varphi(T_w) = 0$ for all the trajectories.

The results in figure 11(b) are overall significantly different for every choice of T_w . However, the more relevant regime for our analysis is the initial one, when $t \ll T_w$. In this regime we observe a linear increase of σ_φ^2 , similarly to that observed in 1D-BM. A zoom of figure 11(b) for the initial regime is shown in figure 12(a). Since when $t \ll T_w$ σ_φ^2 does not depend on T_w (as seen in the figure for $t < 5$ ns) we can calculate a unique value of the phase diffusion coefficient. Figure 12(a) also shows that as T_w increases the range of times in which σ_φ^2 does not depend on T_w is larger.

We now check if the results obtained with our method are in agreement with those obtained with a more conventional method [4, 24]. In [4, 24] the difference in phase fluctuations at times t and $t + \tau$, $\Delta\varphi_\tau(t) = \varphi(t + \tau) - \varphi(t)$, that is a stationary random process, is considered. For each value of τ , the variance of the phase noise, $\sigma_\varphi^2(\tau) = \langle \Delta\varphi_\tau^2(t) \rangle$ can be calculated from the temporal average $\overline{\Delta\varphi_\tau^2(t)}$ because $\langle \Delta\varphi_\tau^2(t) \rangle = \overline{\Delta\varphi_\tau^2(t)}$ because of the stationary character of $\Delta\varphi_\tau(t)$. $\sigma_\varphi^2(\tau)$ is plotted in figure 12(a) when using a time averaging of $100 \mu\text{s}$. This figure shows that there is an excellent agreement between both methods. In this way we calculate the diffusion coefficient, D_φ , by using a linear fitting of the results since $\sigma_\varphi^2 = 2D_\varphi t$ when t is small. The linear fit of the results for $T_w = 1000$ ns in figure 12(a) gives $D_\varphi = 5.57 \pm 0.02 \text{ rad}^2/\text{ns}$ with a regression coefficient of 0.9997.

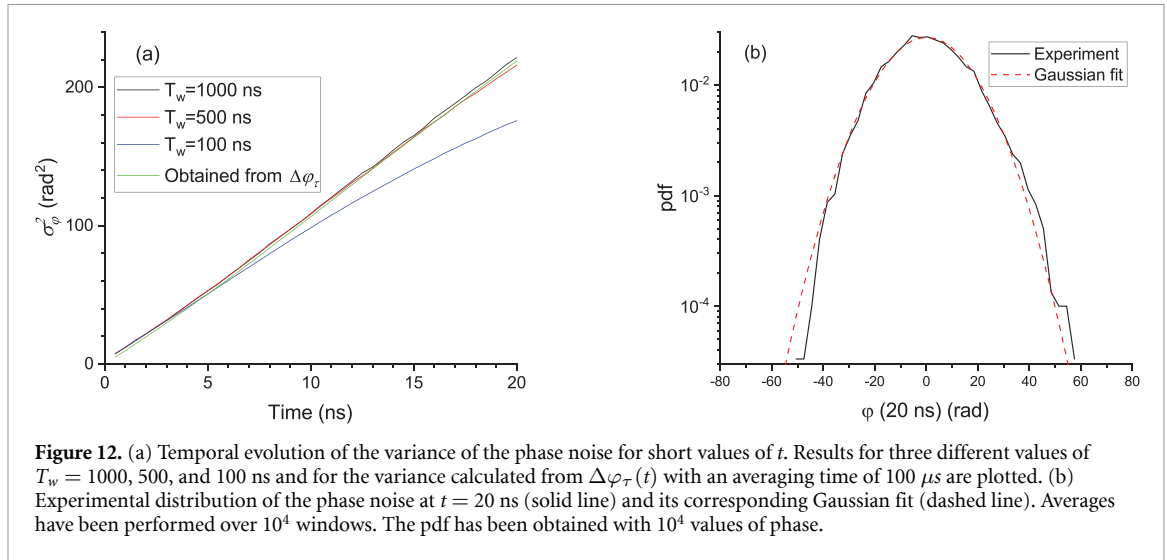


Figure 12. (a) Temporal evolution of the variance of the phase noise for short values of t . Results for three different values of $T_w = 1000$, 500, and 100 ns and for the variance calculated from $\Delta\phi_T(t)$ with an averaging time of 100 μ s are plotted. (b) Experimental distribution of the phase noise at $t = 20$ ns (solid line) and its corresponding Gaussian fit (dashed line). Averages have been performed over 10^4 windows. The pdf has been obtained with 10^4 values of phase.

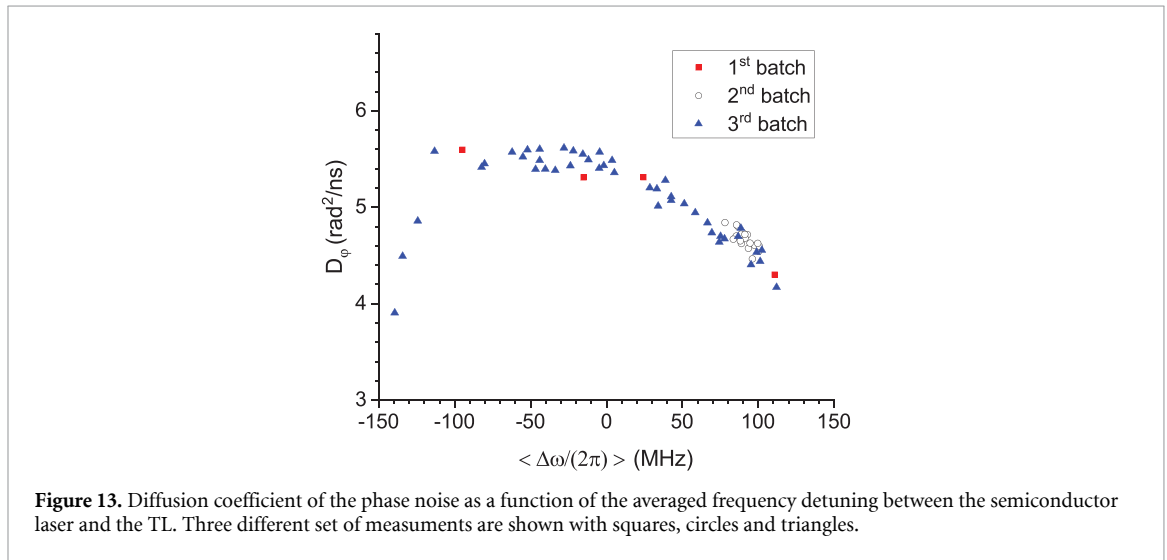


Figure 13. Diffusion coefficient of the phase noise as a function of the averaged frequency detuning between the semiconductor laser and the TL. Three different set of measurements are shown with squares, circles and triangles.

We now consider the distribution of the values of the phase noise in the short time regime $t \ll T_w$. We show in figure 12(b) the experimental distribution of the phase noise at $t = 20$ ns when $T_w = 1000$ ns. The plot also shows the Gaussian distribution obtained with the parameters corresponding to the mean value and standard deviation of the experimental data (0.19 rad and 14.88 rad, respectively). The good agreement found between both distributions indicates that the phase noise measured in this experiment has a Gaussian distribution.

The experimental results that we have shown have been obtained for a single value of the optical wavelength of the TL, λ_{TL} , very close to λ_s since $\langle \Delta\omega/(2\pi) \rangle = -62.2$ MHz. It is then pertinent to investigate the degree of reproducibility of our results and their dependence on λ_{TL} . In order to do that we have performed three different sets of measurements whose results are included in figure 13. In the first batch we have considered four values of λ_{TL} and optical attenuation after the TL in order to have a weaker signal at the oscilloscope ($V_{rms} \approx$ some tens of mV). In the other two batches we have not considered attenuation. In the second batch we have obtained 20 consecutive set of data for a fixed λ_{TL} . In the third batch we have changed λ_{TL} and slight changes of the DML's temperature (smaller than 0.02 $^\circ$ C) to record much more set of data than in the first batch. We have also considered a time separation between different batches of several weeks.

In figure 13 we show the dependence of D_ϕ on $\langle \Delta\omega/(2\pi) \rangle$ that is obtained when changing λ_{TL} under the conditions previously described. The results from batch 1 follow the same trend than the remaining results. This indicate that reproducible results are obtained for very different levels of signal. Also results of batch 2 indicate that, even in the most similar conditions that we can experimentally get, there is some dispersion, but still following the trend of batch 3. The dependence of D_ϕ on $\langle \Delta\omega/(2\pi) \rangle$ becomes clear from the results of batch 3. For $\langle \Delta\omega/(2\pi) \rangle$ between -115 and 25 MHz the value of D_ϕ fluctuates around

a constant value. For the other values of $\langle \Delta\omega/(2\pi) \rangle$ there is a clear decrease of D_φ as the absolute value of $\langle \Delta\omega/(2\pi) \rangle$ increases. The value of D_φ should not depend on λ_{TL} as it is an intrinsic characteristic of the DML laser. Then, in order to have a definite value of D_φ it seems reasonable to consider only the values in the $(-11\ 525)$ MHz interval. In this way we obtain that $D_\varphi = 5.48 \pm 0.10$ rad²/ns.

Phase noise characterization can be performed from the measurement of the laser linewidth by using the heterodyne [42], self-homodyne [43], self-heterodyne [44], delayed self-homodyne [45], delayed self-heterodyne [46, 47], and phase-diversity homodyne and heterodyne receiver [2, 4] methods. An indirect way of obtaining the phase diffusion coefficient from the laser linewidth is to use the Schawlow–Townes–Henry formula [24]. A more direct method for phase noise characterization is to calculate the variance of the phase noise as the temporal average of the squared difference in phase fluctuations at times t and $t + \tau$ [4, 43, 47]. Our method instead calculate the variance of the phase noise by averaging over different trajectories. This has the advantage of a direct calculation of the statistical moments of the phase noise by averaging it over the different trajectories, instead of temporal averaging of a quantity that is not directly the phase noise.

7. Discussion and conclusions

The comparison between experimental and theoretical results must take into account that the theoretical phases are written in the reference frame of the threshold frequency, ω_{th} . This means that the theoretical phase of the laser, $\omega_{th}t + \phi(t)$, must equal the experimental phase, $\omega_s t + \varphi(t)$, obtaining that $\phi(t) = (\omega_s - \omega_{th})t + \varphi(t)$. Since we consider that within each temporal window ω_s is constant, $\phi(t)$ and $\varphi(t)$ differ in a quantity that is not a random variable. In this way the statistical properties of $\phi(t)$ and $\varphi(t)$ must be the same. That is $\sigma_\phi^2 = \sigma_\varphi^2$, and if $\varphi(t)$ is Gaussian, $\phi(t)$ must be Gaussian with a mean value different by a constant $(\omega_s - \omega_{th})t$. As discussed previously, the experimental values obtained with our method are valid in the small time regime, while they do not depend on the chosen temporal window. In that time regime the values of σ_φ^2 depend linearly on time and the probability density function of $\varphi(t)$ approaches a Gaussian. These results are compatible with the predictions of the additive noise model or the 1D-BM. Also, we have not found signs in our experimental results of Cauchy's distributions nor abrupt changes in the values of the phase typical of the multiplicative noise model or the 2D-BM (see figures 1(b), 4(a) or 5(a)). These results indicate that our experimental results are not compatible with the predictions of the multiplicative noise model. As the laser is biased closer to threshold the differences between the theoretical results obtained with the additive and multiplicative models become smaller. In fact, above threshold results are similar because the noise terms in the phase equations for both models become similar.

Stochastic rate equation models such as those used in this work are approximations that worsen as the photon number decreases, that is for bias currents well below the threshold value. A rigorous treatment of spontaneous emission in that limit would require the quantization of the electric field. A proper description would then be given by a quantum mechanical formulation of the rate equations using quantum Langevin terms [48, 49] or master equations [49].

Our proposed experimental method has limitations in practical applications, particularly regarding measurement accuracy as the laser current is decreased well below the threshold value. In this case bandwidth of both, balanced photodetectors and real time oscilloscope, must be increased in order to capture the rapid fluctuations of the generated signals. In our experimental method we have also disregarded the effect of the noise in the photodetectors. On one hand rapid oscillations of the laser's optical field can not be directly resolved by the photodetectors due to their limited bandwidth. On the other hand the amplification stage in our detectors introduce extra noise. In this way our measured value of the diffusion coefficient overestimates the real one and is just an upper bound of its value. Future work will be devoted to introduce post-processing routines based on parametric Wiener filters that have given excellent results in the measurement of laser linewidth even in the presence of strong detector noise [50].

Future work will also be devoted to analyze the experimental dependence of the phase diffusion coefficient on the injected bias current close to threshold to compare with the evolution of the spectral linewidth found in that region [51]. It has been shown [51] that the spectral linewidth of semiconductor lasers is not always a decreasing function of the bias current: lasers with large values of α can have a maximum of the spectral linewidth just above the threshold current. Since the spectral linewidth is directly connected to the phase diffusion coefficient we could also expect some non-monotonous dependence of this coefficient as a function of the bias current. We could also expect that the phase diffusion coefficient in lasers with small values of α , like quantum dot lasers, would decrease as a function of the current. Preliminary experimental results using our method in a DFB laser indicate that the phase diffusion coefficient decreases as the bias current increases when crossing the threshold value. Also experimental Gaussian distributions for

the phase are obtained. The theoretical and experimental analysis of the phase statistics in the pulsed regime will be also the subject of future work.

The additive model works better than the multiplicative model because it has been deduced from first principles [1, 26] for a constant bias current, contrary to the multiplicative one. When the laser is in gain-switching regime there are no derivations from first principles for the additive nor for the multiplicative model. The adopted solution has been to use the multiplicative model since strengths of the noise terms are written in terms of the variables, instead of their averages, making it appropriate for describing the time dependence inherent to gain-switching. However, we remark that this model has not been deduced from first principles and results derived from it can be problematic, like the infinite value of the variance of the optical phase when the bias current is below threshold. Future work will be devoted to the development of new stochastic rate equations models from which finite values of the phase variance are obtained and that can be used in the gain-switching regime.

In summary, we have analyzed theoretically and experimentally the phase noise in semiconductor lasers biased below threshold. The theoretical study has been performed by using two sets of semiconductor laser rate equations, with additive and multiplicative noise terms, that can be approximated by 1-dimensional and two dimensional Brownian motions, respectively, when the laser approaches its steady-state. We have compared the predictions of both models with the results of measurements of the phase noise with a coherent receiver using a 90° optical hybrid. Trajectories, averages and the distribution of the phase noise are experimentally obtained with good agreement with the results obtained with the well established method based on the phase noise difference. Our experimental results have shown that the variance of the phase noise grows linearly in time and has Gaussian statistics, in agreement with the predictions of the model with additive noise, while the main characteristic of the model with multiplicative noise, that is Cauchy's distribution of the phase noise has not been observed. Finally, we have also obtained that the slope of the linear relation between the phase noise variance and time depends on the frequency detuning in the coherent receiver. The measurement of the diffusion coefficient of the phase noise can be performed because we have found that there is a frequency detuning range for which that slope is approximately constant.

Data availability statement

All data that support the findings of this study are included within the article (and any supplementary files).

Acknowledgment

This work was supported by Ministerio de Ciencia e Innovación. PID2021-12345OB-C22 MCIN/AEI/10.13039/501100011033/FEDER,UE. Authors would like to thank Ignacio Esquivias, Bryan Kelleher, and Paula Pérez.

Conflict of interest

All authors declare that they have no conflicts of interest.

ORCID iD

Angel Valle  <https://orcid.org/0000-0002-3307-5485>

References

- [1] Henry C 1986 *J. Lightwave Technol.* **4** 298–311
- [2] Kikuchi K 2015 *J. Lightwave Technol.* **34** 157–179
- [3] O'Carroll J, Phelan R, Kelly B, Byrne D, Barry L P and O'Gorman J 2011 *Opt. Express* **19** B90–B95
- [4] Kikuchi K 2012 *Opt. Express* **20** 5291–5302
- [5] Wu Y, Deng L, Yang K and Liang W 2022 *IEEE Photonics Technol. Lett.* **34** 1123–1126
- [6] Li J, Yu Z, Du Z, Ji Y and Liu C 2020 *Remote Sens.* **12** 2771
- [7] Geng J, Spiegelberg C and Jiang S 2005 *IEEE Photonics Technol. Lett.* **17** 1827–1829
- [8] Xu F, Ma X, Zhang Q, Lo H-K. and Pan J-W. 2020 *Rev. Mod. Phys.* **92** 025002
- [9] Paraíso T K, Woodward R I, Marangon D G, Lovic V, Yuan Z and Shields A J 2021 *Adv. Quantum Technol.* **4** 2100062
- [10] Alkhazragi O, Lu H, Yan W, Almaymoni N, Park T-Y, Wang Y, Ng T K and Ooi B S 2023 *Ann. Phys.* **2300289** 535
- [11] Currás-Lorenzo G, Nahar S, Lütkenhaus N, Tamaki K and Curty M 2023 *Quantum Sci. Technol.* **9** 015025
- [12] Stipčević M and Koç ÇK 2014 True random number generators *Open Problems in Mathematics and Computational Science* (Springer) 275–315
- [13] Ma X, Yuan X, Cao Z, Qi B and Zhang Z 2016 *npj Quantum Inf.* **2** 1–9
- [14] Herrero-Collantes M and García-Escartín J C 2017 *Rev. Mod. Phys.* **89** 015004

- [15] Jofre M, Curty M, Steinlechner F, Anzolin G, Torres J, Mitchell M and Pruneri V 2011 *Opt. Express* **19** 20665–20672
- [16] Abellán C, Amaya W, Jofre M, Curty M, Acín A, Capmany J, Pruneri V and Mitchell M 2014 *Opt. Express* **22** 1645–1654
- [17] Yuan Z, Lucamarini M, Dynes J, Fröhlich B, Plews A and Shields A 2014 *Appl. Phys. Lett.* **104** 261112 2014
- [18] Abellán C, Amaya W, Domenech D, Muñoz P, Capmany J, Longhi S, Mitchell M W and Pruneri V 2016 *Optica* **3** 989–994
- [19] Marangon D G *et al* 2024 *Nat. Electron.* 1–9
- [20] Loudon R 2000 *The Quantum Theory of Light* (OUP Oxford)
- [21] Lovic V, Marangon D G, Lucamarini M, Yuan Z and Shields A J 2021 *Phys. Rev. Appl.* **16** 054012
- [22] Shakhovoy R *et al* 2023 *Phys. Rev. A* **107** 012616
- [23] Quirce A and Valle A 2021 *Opt. Express* **29** 39473–39485
- [24] Agrawal G P and Dutta N K 2013 *Semiconductor Lasers* (Springer)
- [25] Coldren L A, Corzine S W and Mashanovitch M L 2012 *Diode Lasers and Photonic Integrated Circuits* vol 218 (Wiley)
- [26] Lax M and Louisell W 1969 *Phys. Rev.* **185** 568
- [27] Septriani B, de Vries O, Steinlechner F and Gräfe M 2020 *AIP Adv.* **10** 055022
- [28] Shakhovoy R, Sharoglazova V, Udaltsov A, Duplinskiy A, Kurochkin V and Kurochkin Y 2021 *IEEE J. Quantum Electron.* **57** 1–7
- [29] Quirce A and Valle A 2022 *Opt. Laser Technol.* **150** 107992
- [30] Valle A 2023 *Phys. Rev. Appl.* **19** 054005
- [31] Balle S, De Pasquale F, Abraham N and San Miguel M 1992 *Phys. Rev. A* **45** 1955–1966
- [32] Spano P, D'Ottavi A, Mecozzi A, Daino B and Piazzolla S 1989 *IEEE J. Quantum Electron.* **25** 1440–1449
- [33] Petermann K 1991 *Laser Diode Modulation and Noise* vol 3 (Springer Science & Business Media)
- [34] Rosado A, Pérez-Serrano A, Tijero J M G, Valle A, Pesquera L and Esquivias I 2019 *IEEE J. Quantum Electron.* **55** 2001012
- [35] Lévy M P 1940 *Am. J. Math.* **62** 487–550
- [36] Spitzer F 1958 *Trans. Am. Math. Soc.* **87** 187–197
- [37] Riskin H 1996 *The Fokker-Planck Equation* (Springer)
- [38] Kloeden P E and Platen E 1992 *Stochastic differential equations Numerical Solution of Stochastic Differential Equations* (Springer)
- [39] Quirce A, Rosado A, Díez J, Valle A, Pérez-Serrano A, Tijero J M G, Pesquera L and Esquivias I 2020 *IEEE Photon. J.* **12** 1–14
- [40] Gardiner C W *et al* 1985 *Handbook of stochastic methods* 3 (Springer)
- [41] Igarashi K, Kiwata H, Kikuta M and Shigihara M 2021 *J. Lightwave Technol.* **39** 6539–46
- [42] Young B, Cruz F, Itano W and Bergquist J 1999 *Phys. Rev. Lett.* **82** 3799
- [43] Attia I, Wohlgemuth E, Balciano O, Cohen R J, Yoffe Y and Sadot D 2022 *Opt. Express* **30** 14492–504
- [44] Kueng A, Thevenaz L and Robert P A 1996 Laser linewidth determination in the sub-megahertz range using a Brillouin fibre laser *Proc. European Conf. on Optical Communication* vol 2 (IEEE) 305–308
- [45] Nazarathy M, Sorin W V, Baney D M and Newton S A 1989 *J. Lightwave Technol.* **7** 1083–1096
- [46] Okoshi T, Kikuchi K and Nakayama A 1980 *Electron. Lett.* **16** 630–631
- [47] Huynh T N, Nguyen L and Barry L P 2011 *IEEE Photon. Technol. Lett.* **24** 249–251
- [48] Lax M 1966 *Phys. Rev.* **145** 110
- [49] Gardiner C and Zoller P 2004 *Quantum Noise: A Handbook of Markovian and Non-Markovian Quantum Stochastic Methods with Applications to Quantum Optics* (Springer)
- [50] Kantner M and Mertenskötter L 2023 *Opt. Express* **31** 15994–16009
- [51] Toffano Z 1997 *IEEE J. Sel. Top. Quantum Electron.* **3** 485–490